Materials Transactions, Vol. 49, No. 11 (2008) pp. 2723 to 2727

EXPRESS REGULAR ARTICLE

Formation of Porous Intermetallic Thick Film by Ni-Al Microscopic Reactive Infiltration

Tatsuya Ohmi, Naoya Hayashi* and Manabu Iguchi

Division of Materials Science and Engineering, Graduate School of Engineering, Hokkaido University, Sapporo 060-8628, Japan

Microporous structures of nickel-aluminide thick films lining the inner wall of microchannels have been investigated. The microchannels were produced in metal bodies by a powder metallurgical process utilizing microscopic reactive infiltration. In the experiment, a nickel-powder compact containing shaped aluminum wires was sintered at a temperature between the melting points of nickel and aluminum. Infiltration and diffusion of aluminum into the surrounding nickel powder, accompanied by the reaction between the metals, occurred during the sintering and brought about the formation of microchannels lined with a NiAl intermetallic layer. In this process, nickel powder composed the device body, and the aluminum wires gave the shape of the microchannels. The intermetallic layer had a microporous structure when the diameter of the aluminum wire was 500 μm and the porosity of the compact specimen was 23.6–31.5% within the porosity range examined. When the porosity was 36.0%, such a structure, the porous thick film, was not observed. On the other hand, the porous NiAl thick film was produced in all specimens with an aluminum wire of 200 μm in diameter. The voidage of the porous thick film was maximized when the porosity of the compact specimen was 29.8%, and it reached to 53.8% in the case the diameter of the aluminum wire was 500 μm, and 60.2% in the case that was 200 μm.
[doi:10.2320/matertrans.MER2008188]

(Received June 10, 2008; Accepted August 19, 2008; Published October 8, 2008)

Keywords: *microporous structure, thick film, intermetallic compound, nickel aluminide, microchannel, reactive infiltration, powder metallurgy, microreactor, catalyst support*

1. Introduction

In recent years, the development of metallic microreactors for catalytic reactions has been investigated actively.[1–9] The high surface to volume ratio of the microreactor is suitable for catalytic reaction. In addition, the high heat transfer because of the microchannel structure and good heat conductivity of metals allows keeping the reaction temperature throughout the reactor even if the reaction is highly exothermic or endothermic. Furthermore, it enables fast heating and cooling of reactants in open reactor systems.

The metallic materials which were examined for the catalyst support or substrate in the previous reports are stainless steel,[1–3] Fe-Cr-Al alloy,[4,5] aluminum,[6–8] and so on. Meille[9] presented a detailed review on methods to deposit catalysts on structured surfaces, and listed the materials for the structure including these metals. The target reactions were also varied. Rebrov *et al.*[1] reported a stainless steel microreactor for catalytic reduction of nitric oxide with ammonia by a zeolite catalyst. Aartun *et al.*[4] described catalytic conversion of propane to hydrogen in Fe-Cr-Al alloy microreactors with Ni or Rh catalyst. Pfeifer *et al.*[7] examined aluminum microreactors with PdZn catalysts for methanol steam reforming. In most of these previous studies, microchannels were produced by methods of manufacturing structured surfaces. The workpieces with the structured surfaces were put one on top of the other, and then their matching surfaces were sealed. Such a process will take extended processing time and much cost. From a practical viewpoint, methods of fabricating microchannels directly in bulk metals would be more beneficial. Recently, we proposed a powder-metallurgical microchanneling process and demonstrated its feasibility.[10–12] The concept for the process we proposed is based on a microscopic infiltration phenomenon that often occurs during liquid phase sintering of a mixture of powder metals with different melting points. We call the metal with higher melting point the body metal, which is to compose the device body, and another the sacrificial-core metal, which is to give the shape of the microchannel. Figure 1 depicts the expected microchanneling mechanism. In this process, a body-metal powder compact containing shaped sacrificial-core metal is sintered at a temperature between the melting points of these metals. During sintering of the powder compact, molten sacrificial-core metal migrates to the body-metal powder region by infiltration and diffusion. In many cases, these metals react and produce an intermetallic liner surrounding the cavity formed at the sites initially occupied by the sacrificial core. In these cases, the sacrificial core acts as an element source for the resulting intermetallic liner.

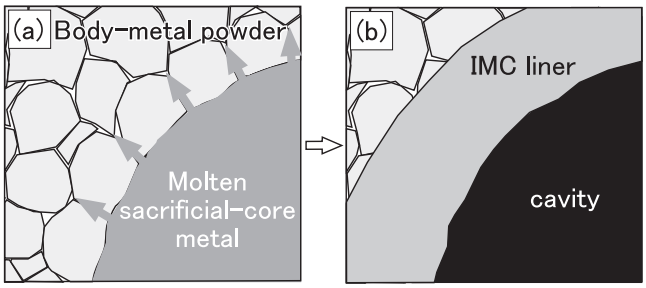

Fig. 1 Schematic representation of the microchannel formation mechanism.

In the course of our study, we found that a Ni-Al intermetallic thick film formed as a liner of the microchannel when we used nickel and aluminum as the body metal and the sacrificial-core metal, respectively. The thick film consisted of NiAl, and in some cases it had microporous structure. Considering the good heat resistance, high thermal conductivity and excellent corrosion resistance of NiAl,[13] such a porous thick film seemed to be suitable for a catalyst support or substrate. In the present study, therefore, we

*Graduate Student, Hokkaido University

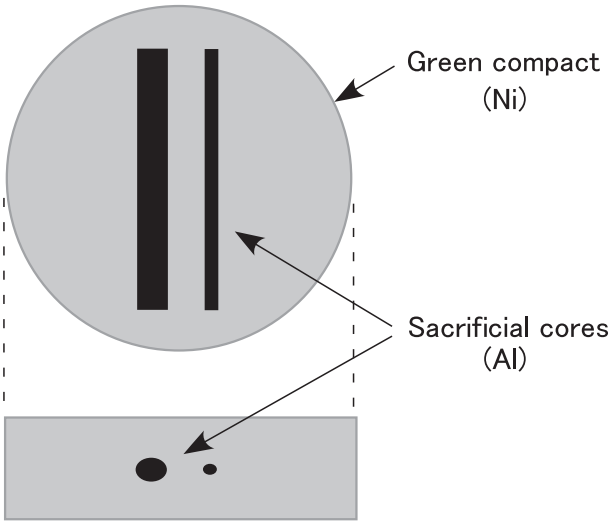

Fig. 2 Schematic illustration of the green compact.

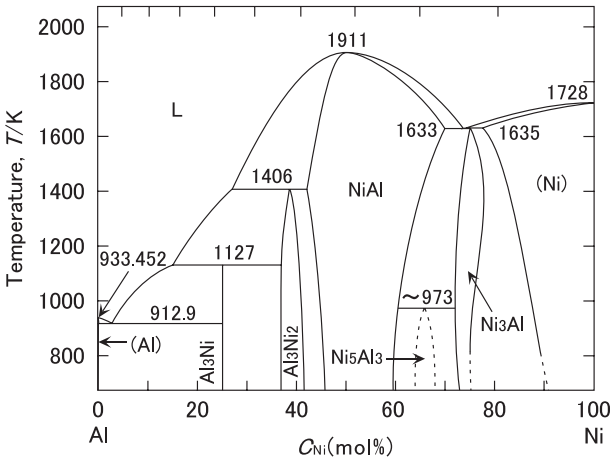

Fig. 3 Al-Ni binary alloy phase diagram.[14]

investigated process parameters to control the structure of the thick film, especially focusing on the porosity of the powder compact and the diameter of the sacrificial core.

2. Experimental Procedure

A nickel powder compact containing aluminum sacrificial cores was sintered in an argon atmosphere at a temperature between the melting points of aluminum and nickel. The average diameter of the nickel powder particles was 5 μm. The shape of the sacrificial core was a wire 200 or 500 μm in diameter and 15 millimeters in length. Thirteen grams of nickel powder and two sacrificial cores with different diameters were cold-pressed into a cylindrical green compact in a metal mold using a unidirectional pressure in the range from 300 to 760 MPa. The resulted green compact had a diameter of 20 mm and height of about 5 mm, and its porosity was varied from 23.6 to 36.0% depending on the pressing pressure. Figure 2 schematically illustrates the green compact. The initial cross section of each wire was round; however, the wires were distorted into a slightly oblate figure by unidirectional pressing as illustrated in Fig. 2. Figure 3 shows an Al-Ni binary alloy phase diagram.[14] The green compact specimen was heated at a constant rate of $0.2\,K{\cdot}s^{-1}$ from room temperature to 1473 K, and then furnace-cooled at about $0.4\,K{\cdot}s^{-1}$. The maximum temperature, 1473 K, is 540 K higher than the melting point of aluminum, and within the range of the sintering temperature commonly used in the powder metallurgy of nickel.

3. Results and Discussion

3.1 Structure evolution around the microchannel

Figure 4 presents examples of the back-scattered electron (BSE) images of the structures near the microchannels formed in the sintered specimens with initial porosity of 36.0, 29.8 and 23.6%. The diameter of the sacrificial core, d, was 500 μm in each photograph. In all the specimens fabricated in our experiments, open microchannels were produced. However, the structure of the reaction-product region around the microchannel depended on the porosity of the green compact as shown in Fig. 4. In Figs. 4(b) and 4(c), there are thick films with almost uniform thickness and a peculiar porous structure in which long and thin micropores have grown along the thickness direction of the film. In contrast, such a porous thick film was not observed in the specimen shown in Fig. 4(a). Instead, there is a reactive-infiltrated region which has irregularly spread into the nickel powder region in this specimen. Similar but much smaller reactive-infiltrated region can be seen in Fig. 4(b). In Fig. 4(c), similar region is observed along the cracks which advanced toward the nickel powder region. These results indicate that the porous thick film acted as a kind of a permeable (or partially permeable) wall which controls the infiltration of the liquid aluminum into the nickel powder region, and that the liquid aluminum leaked out when a part of the thick film broke. In fact, our previous work[15] revealed that a molten sacrificial core still remained at 1273 K in a specimen with a relatively low porosity (20.1%). Figure 5 depicts the structure near the sacrificial core in the specimen quenched at 1273 K in the course of sintering.[15] In the figure, an Al_3Ni_2 thick film surrounds a solidification structure which consists of intermetallic facet dendrites and an aluminum solid solution matrix. This solidification structure was formerly a molten sacrificial core before quenching.

It is also worth noting that long and thin micropores like those in the porous thick film were not observed in a freely reactive-infiltrated region. This result may give a suggestive hint for the mechanism of porous thick film formation. For a more detailed discussion, however, we have to valuate the wettability of the liquid aluminum (alloy) against the equilibrium intermetallic phase, *i.e.*, Al_3Ni, Al_3Ni_2 or NiAl, which changes depending on the temperature (see Fig. 3). The change of solid volume, which is caused by the reactive infiltration and subsequent solid-phase transformations, also should be clarified. Those will be the subjects for future investigation.

3.2 Structure of the porous thick film

Figure 6(a) shows a typical structure of the porous thick film, and Fig. 6(b) illustrate the aluminum-concentration profile measured by EPMA along the line A-B drawn in

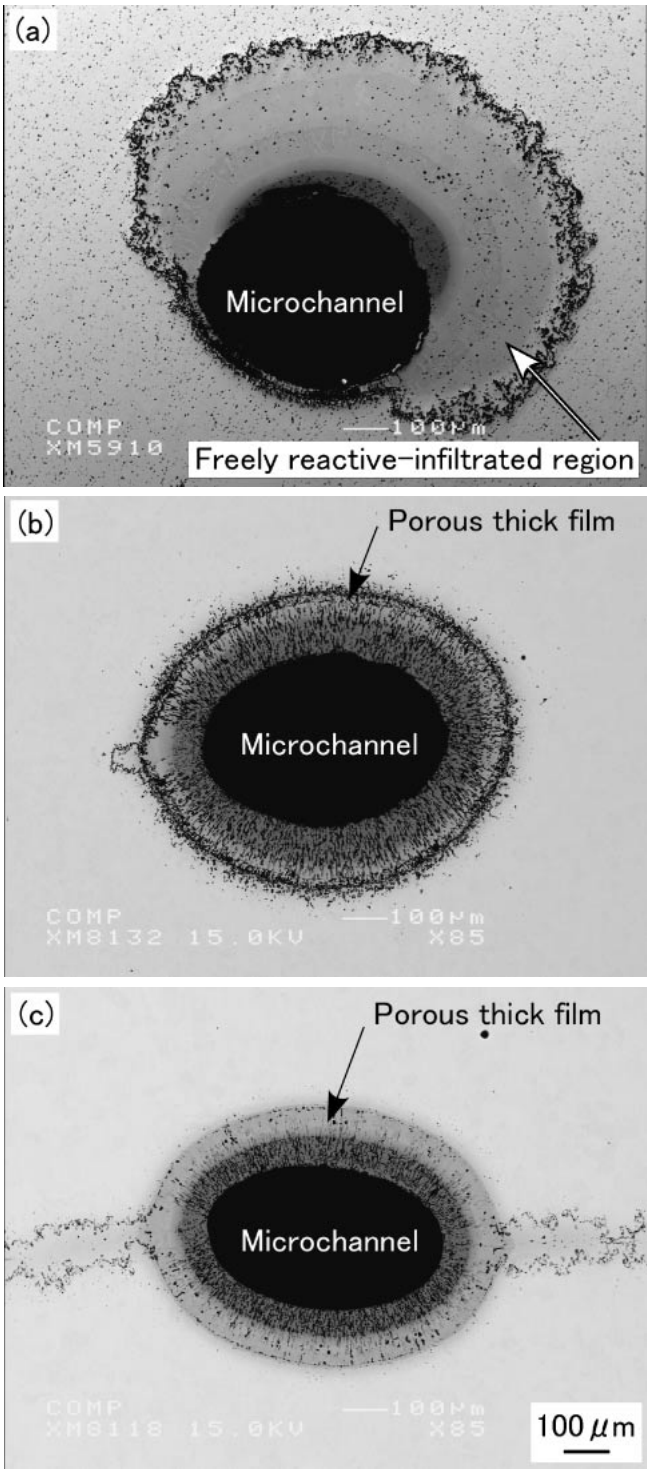

Fig. 4 Back-scattered electron images of the structures near the microchannels ($d = 500\,\mu m$). Porosity of the green compact: (a) 36.0%, (b) 29.8%, and (c) 23.6%. In these images, the brightness difference represents the difference in nickel concentration.

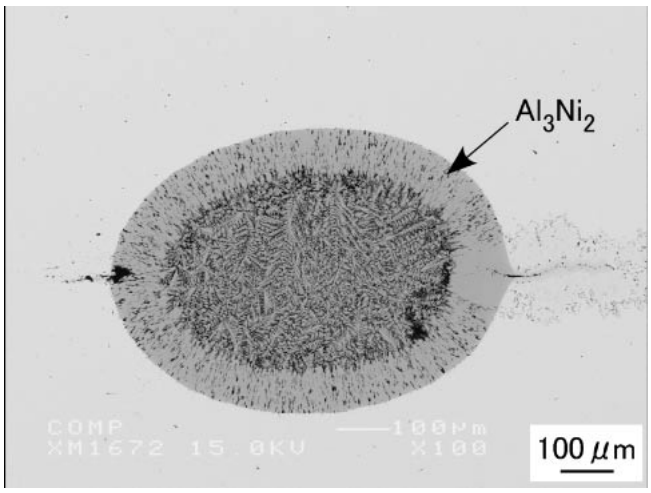

Fig. 5 Structure near the sacrificial core ($d = 500\,\mu m$) in the specimen quenched at 1273 K in the course of sintering.[15)]

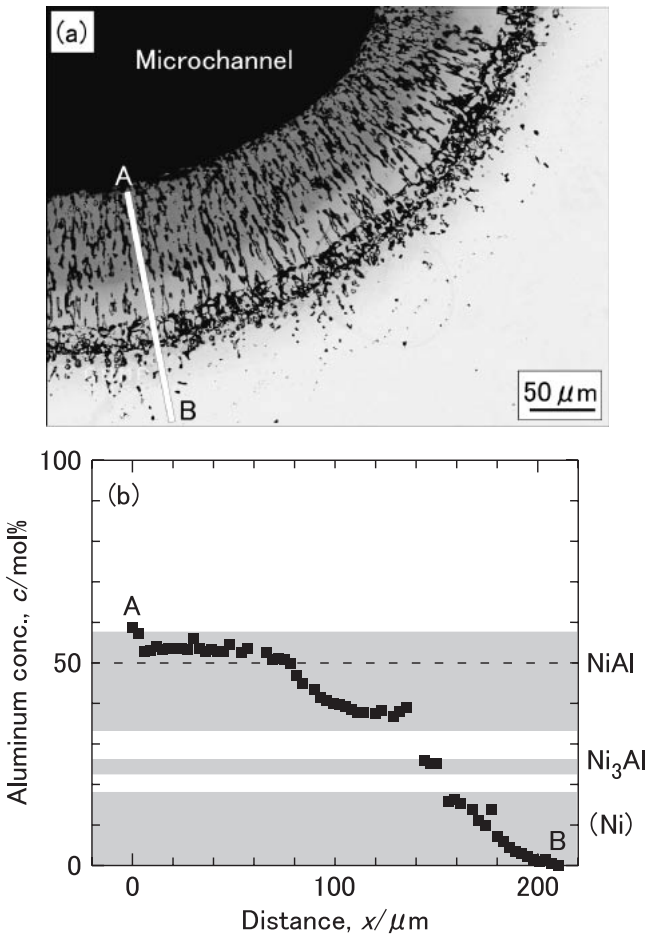

Fig. 6 Structure of the porous thick film (a) and aluminum-concentration profile along the line A-B (b). Porosity of the green compact was 29.8% and $d = 500\,\mu m$. The gray bands drawn on the concentration profile indicate the composition ranges of NiAl, Ni_3Al, and nickel solid solution at 1473 K.

Fig. 6(a). The brightness contrast in Fig. 6(a) indicates that the porous thick film is constructed in a concentric configuration and consists of two sub-layers. The average aluminum concentration was 53.5 mol% in the innermost sub-layer (from $x = 0$ to 77 μm) and 40.5 mol% in the second sub-layer (from $x = 77$ to 140 μm). Such a pseudo phase-separation into an Al-rich NiAl ($NiAl_{Al}$) region and a Ni-rich NiAl ($NiAl_{Ni}$) region has often been observed in Ni-Al diffusion-couple experiments; it is caused by a non-proportional composition dependence of the diffusion coefficient in the NiAl phase.[16)] Another noteworthy fact is that the $NiAl_{Al}$ sub-layer is much porous than the $NiAl_{Ni}$ sub-layer. Figure 7

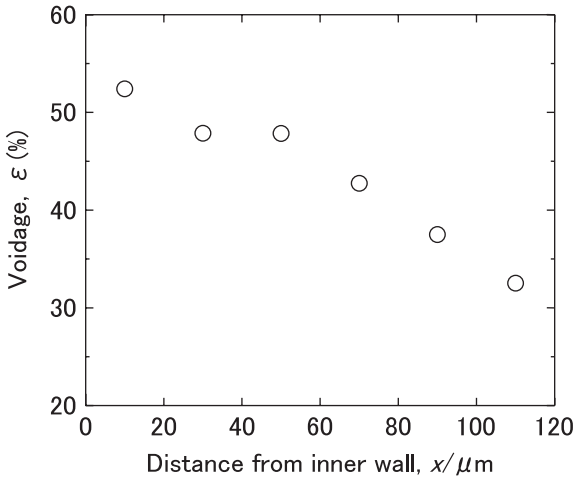

Fig. 7 Voidage distribution in the porous thick film in the specimen shown in Fig. 6.

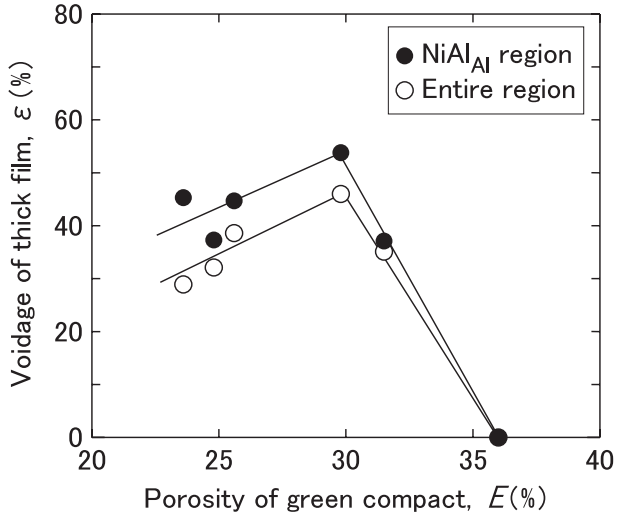

Fig. 8 Relationship between the porosity of the green compact and the voidage of the thick film when $d = 500\,\mu m$.

presents a voidage distribution in a NiAl porous thick film. The voidage was measured by image analysis on the BSE image of the characteristically porous region. In Fig. 7, there is a graded distribution in which the voidage decreases with distance from the inner wall of the microchannel. Such a distribution is suitable for catalyst supports. Similar structure was observed in all the thick films produced with a 500 μm-diameter sacrificial core.

Figure 8 depicts the relationship between the porosity of the green compact and the voidage of the thick film in the case the diameter of the sacrificial core was 500 μm. The average voidage of the entire region of the NiAl thick film maximized when the porosity of the green compact specimen was 29.8%, and it reached to 46.0%. For the $NiAl_{Al}$ sub-layer, the maximum voidage was 53.8%.

3.3 Influence of the sacrificial-core diameter

Figure 9 shows the BSE images of the structures near the microchannels produced with 200 μm-diameter sacrificial cores. There are two noticeable differences betweens the

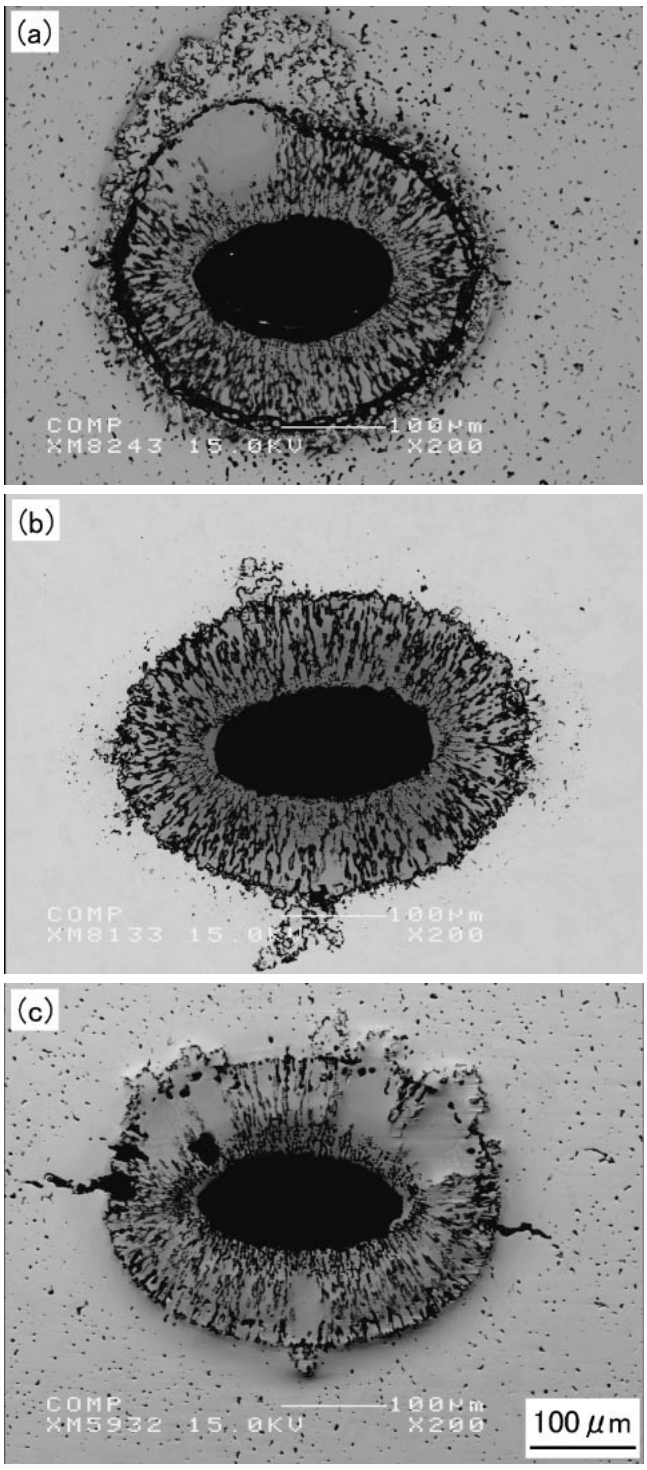

Fig. 9 Structures near the microchannels ($d = 200\,\mu m$). Porosity of the green compact: (a) 36.0%, (b) 29.8%, and (c) 23.6%.

results of 200 μm- and 500 μm-diameter sacrificial cores. As for phase constitution, EPMA results showed that the porous thick films consisted of only $NiAl_{Ni}$ layer in all the cases when $d = 200\,\mu m$. This resulted from rapid Al-diffusion out of the thick film with a higher specific surface area. Another difference from the case of the 500 μm-diameter sacrificial core is that a porous thick film formed even when the green-compact porosity was 36.0%. The reason for this is probably because the porous intermetallic film was sturdier than that in the case of the 500 μm-diameter sacrificial core. The

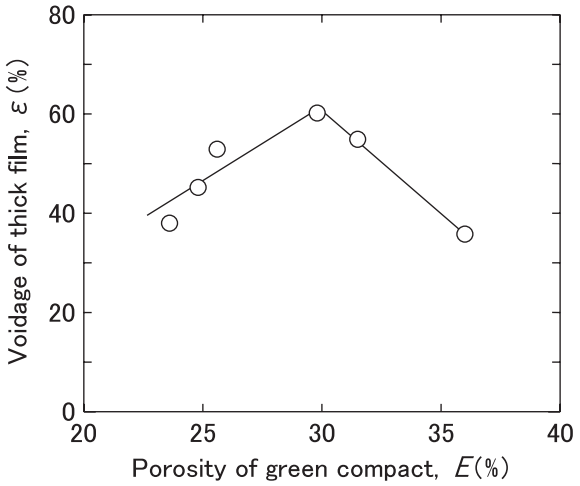

Fig. 10 Relationship between the porosity of the green compact and the voidage of the thick film when $d = 200\,\mu m$.

ratio of the thickness of the porous intermetallic film to the size of the microchannel, which was formerly a liquid-aluminum pool, was about 0.45 when $d = 200\,\mu m$ and about 0.25 when $d = 500\,\mu m$. The porous intermetallic film in the case of Fig. 10(a) probably was sturdy enough to prevent a massive leaking of liquid aluminum.

Figure 10 illustrates the relationship between the porosity of the green compact and the voidage of the thick film in the case when $d = 200\,\mu m$. The voidage was maximized when the porosity of the green compact was 29.8%, as in the case when $d = 500\,\mu m$. The maximum voidage was 60.2% which is higher than that in the case of the 500 μm sacrificial core.

The above results, especially those shown in Fig. 4, indicate that evolution of the microporous structure in the intermetallic liner relates closely to the microchanneling mechanism, and it is certain that many factors including capillarity, diffusion, phase transformation and reaction come into play in the microchannel formation. In the present study, we found the optimum conditions for producing microporous intermetallic thick film. The mechanism of its formation is the subject to be investigated in the future.

4. Conclusions

We found the formation of a porous thick film of NiAl intermetallic compound surrounding a microchannel and investigated the influence of two process parameters, the porosity of the powder compact and the diameter of the sacrificial core, on the structure of the thick film. The results of our investigation are summarized as follows.

(1) The thick film has a microporous structure when the diameter of the sacrificial core was 500 μm and the porosity of the compact specimen was 23.6–31.5%. The thick film has almost uniform thickness and a peculiar porous structure in which long and thin pores have grown along the thickness direction of the film.

(2) When the diameter of the sacrificial core was 500 μm and the porosity of the compact specimen was 36.0%, a massive leaking of liquid aluminum occurred and an irregularly-spread reactive-infiltrated region was produced. The reactive-infiltrated region in this case has no such micropores that observed in the porous thick film.

(3) When the diameter of the sacrificial core was 200 μm, porous thick films were produced in all specimens.

(4) The porous thick film consists of two sub-layers, *i.e.*, an Al-rich NiAl sub-layer and a Ni-rich NiAl sub-layer, when the diameter of the sacrificial core was 500 μm. The former sub-layer is much porous than the latter one. When the diameter of the sacrificial core was 200 μm, the porous thick film consists of only one layer of Ni-rich NiAl phase.

(5) In both cases of 500 μm- and 200 μm-diameter sacrificial cores, the voidage of the thick film is maximized when the porosity of the green compact was 29.8%.

Acknowledgement

This work was partly supported by a grant from the JFE 21 Century Foundation and KAKENHI (C) (19560740).

REFERENCES

1) E. V. Rebrov, G. B. F. Seijger, H. P. A. Calis, M. H. J. M. de Croon, C. M. van den Bleek and J. C. Schouten: Applied Catalysis A: General **206** (2001) 125–143.
2) G.-G. Park, D. J. Seo, S.-H. Park, Y.-G. Yoon, C.-S. Kim and W.-L. Yoon: Chem. Eng. J. **101** (2004) 87–92.
3) G. Chen, Q. Yuan, H. Li and S. Li: Chem. Eng. J. **101** (2004) 101–106.
4) I. Aartun, T. Gjervan, H. Venvik, O. Görke, P. Pfeifer, M. Fathi, A. Holmen and K. Schubert: Chem. Eng. J. **101** (2004) 93–99.
5) I. Aartun, B. Silberova, H. Venvik, P. Pfeifer, O. Görke, K. Schubert and A. Holmen: Catalysis Today **105** (2005) 469–478.
6) E. V. Rebrov, M. H. J. M. de Croon and J. C. Schouten: Catalysis Today **69** (2001) 183–192.
7) P. Pfeifer, K. Schubert, M. A. Liauw and G. Emig: Applied Catalysis A: General **270** (2004) 165–175.
8) C. Fukuhara, Y. Kamata and A. Igarashi: Applied Catalysis A: General **296** (2005) 100–107.
9) V. Meille: Applied Catalysis A: General **315** (2006) 1–17.
10) T. Ohmi, K. Matsuura and M. Kudoh: Int. J. Self-Propagating High-Temp. Synthesis **13** (2004) 121–129.
11) T. Ohmi, M. Takatoo, M. Iguchi, K. Matsuura and M. Kudoh: Mater. Trans. **47** (2006) 2137–2142.
12) T. Ohmi, M. Sakurai, K. Matsuura, M. Kudoh and M. Iguchi: Int. J. Transport Phenomena **9.2** (2007) 105–111.
13) R. Darolia: J. Met. **43** (1991) 44–49.
14) H. Okamoto: *Binary Alloy Phase Diagrams (2nd. ed., Plus Updates)*, [CD-ROM, ver.1.0] (ASM International, Materials Park, 1996).
15) T. Ohmi, M. Sakurai, K. Matsuura, M. Kudoh and M. Iguchi: Functionally Graded Materials **19** (2005) 103–108.
16) M. Watanabe, Z. Horita and M. Nemoto: Defect and Diffusion Forum **143–147** (1997) 637–642.